A Locally Adaptive Region Growing Algorithm for Vascular Segmentation

Jaeyoun Yi, Jong Beom Ra

Department of Electrical Engineering and Computer Science, Korea Advanced Institute of Science and Technology (KAIST), 373-1, Guseong-dong Yuseong-gu, Daejeon 305-701, ROK

Received: 1 June 2003; accepted 30 October 2003

ABSTRACT: To segment vascular structures in 3-D CTA/MRA images, this article presents a new region growing algorithm based on local cube tracking. In the proposed algorithm, a small local cube is segmented to detect a vessel segment, and the following local cube(s) is determined based on the segmentation result. This procedure is repeated until the segmentation is completed. By confining the segmentation inside each local cube, a robust result can be obtained even in a tubular structure of steadily changing intensity. For segmentation, a locally adaptive and competitive region growing scheme is adopted to obtain well-defined vessel boundaries. It should be emphasized that the proposed algorithm can detect all branches with practically acceptable computational complexity. In addition, its segmentation result is represented as a tree structure having many branches so that a user may easily correct the result branch-by-branch, if necessary. Experimental results from real images prove that the proposed algorithm produces prospective vessel segmentation results for 3-D CTA/MRA images and segments vessels of various sizes well, including stenoses and aneurysms. © 2003 Wiley Periodicals, Inc. Int J Imaging Syst Technol, 13, 208–214, 2003; Published online in Wiley InterScience (www.interscience.wiley.com). DOI 10.1002/ima.10059

Key words: vessel segmentation; locally adaptive region growing; competitive region growing; local cube tracking; tree-structured segmentation

I. INTRODUCTION

Because of the rapid development of 3-D imaging modality and related software, 3-D medical images are actively used in various advanced medical systems, such as surgical simulators, computer-aided diagnosis systems, and computer-assisted surgery systems. To maximally utilize the 3-D image information in those systems, however, the segmentation of various human organs is usually required. In particular, an accurate description of vessel structures in 3-D images is very important in many clinical applications, e.g., quantitative diagnosis, surgical planning, and monitoring of disease progress or remission (Wilson and Noble, 1999; Wink et al., 2000; Bhalerao et al., 2001).

Therefore, various algorithms have been proposed to segment vessels from 3-D medical images, such as CT angiography (CTA) and MR angiography (MRA) in which vessels are enhanced to have higher intensity values. Model-based algorithms segment vessel structures by assuming that their shapes can be represented by generalized cylinders, B-splines, or triangulated surfaces (Verdonck et al., 1996; O'Donnel et al., 1997; Terzopoulos et al., 1988, Fiebich et al., 1997). In these algorithms, intensive research has been focused on the multi-scale analyses of high order derivative operators like the *Hessian* matrix to detect tubular structures in 3-D space (Lorenz et al., 1997; Krissian et al., 1998; Koller et al., 1995; Prinet and Monga, 1997; Furst et al., 1996). These algorithms are able to cope with varying widths of vessels by adopting multiscale analyses in principle. However, they have an inherent risk of missing abnormalities, for example, aneurysms and stenoses, because the models are based on the normal shape of vessels. Furthermore, their heavy computation is noticed as a practical drawback.

Assuming that the intensity values of vessels are in a distinguishing range, threshold-based algorithms have been widely used in practical applications (Felkel and Wegenkittl, 2001). They choose the desired connected components after a binary volume is generated by applying either automatic or manual threshold values. It is obvious that these algorithms do not cope with local intensity variation in 3-D space if a single global threshold value is applied to the whole volume. To compensate for this problem, an adaptive segmentation algorithm has been proposed for time-of-flight (TOF) MRA images (Wilson and Noble, 1999). In this algorithm, the thresholding parameter is estimated recursively on smaller subvolumes of data so that the best model is found for each localized region, by assuming that the intensity distribution is a mixture of *Gaussian* distributions. However, it can be applied only to TOF-MRA images, in which vessels have the highest intensity values compared to those of other tissues.

A fast central axis tracking algorithm has been proposed using a new center-likelihood measure (Wink et al., 2000). The algorithm is very robust to abnormalities, and it can produce accurate centerlines for vessels very fast because it does not search the whole volume data but the candidate planes only. Although a "search-tree" has been introduced as an extension in the article to cover branching cases, the algorithm cannot manage every branching case because the center-likelihood function ignores perpendicularly outgoing branches. A new algorithm that uses iterative tracking of vessel

Correspondence to: J.-B. Ra; E-mail: jbra@ee.kaist.ac.kr

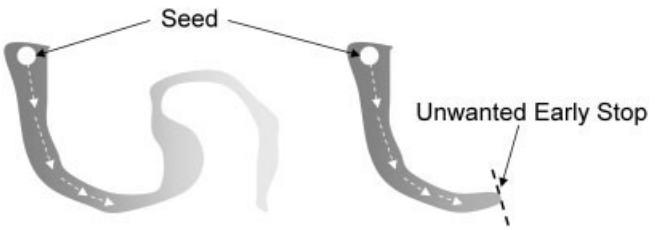

Figure 1. Even slow intensity variation may cause an unwanted stop of the region growing process in vascular structures.

centerlines has been proposed to detect all branches inside each local parallelepiped (Flasque et al., 2001). However, this algorithm is also preceded by a thresholding algorithm, so it is not adaptive to local intensity variation.

In most cases of image segmentation, region growing procedures (Adams and Bischof, 1994; Hojjatoleslami and Kittler, 1998; Gonzalez and Woods, 1993) usually produce well-defined object boundaries if the intensity change inside the object of interest is not considerable. However, in vascular structures that consist of very long and narrow pipe-like objects, even slow intensity variation may cause an unwanted stop of the region growing process unless the parameters used for homogeneity test are adaptively adjusted (see Fig. 1). Recently, the concept of fuzzy-connectedness has also been employed to segment vessels (Saha et al., 2000; Lei et al., 2000).

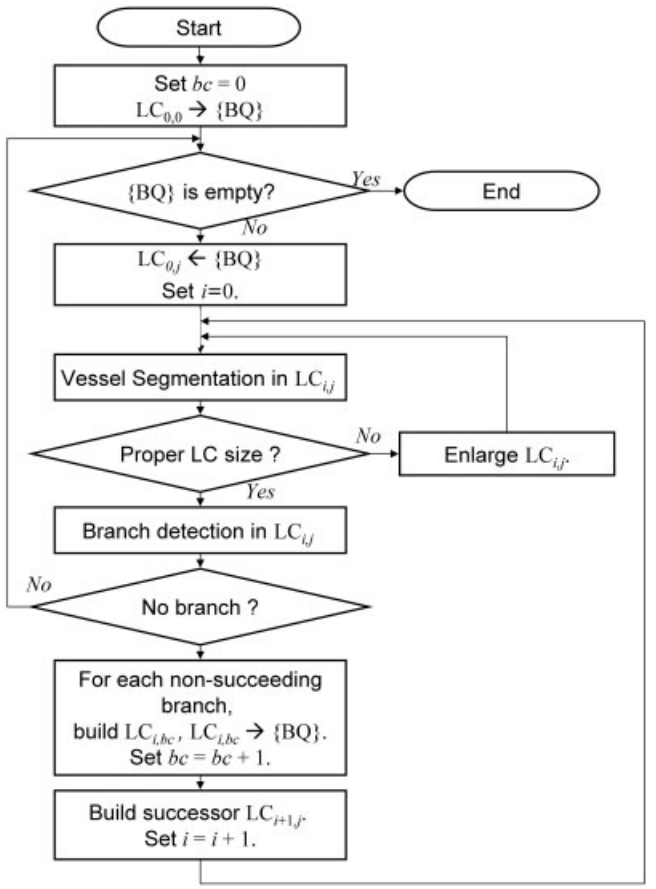

Figure 2. Flow chart of the proposed algorithm.

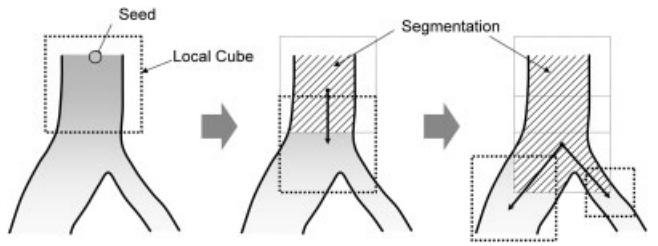

Figure 3. Local cube tracking. It is depicted in the 2-D space for simplicity.

Although local fuzzy affinity is used in fuzzy connectedness, the final segmentation is usually acquired by adjusting a single global parameter interactively. Hence, it may not be proper for the segmentation of a long vessel with slow intensity variation, which is not unusual in CTA.

In this article, we propose a new region growing algorithm based on local cube tracking. The algorithm confines the region growing process to each local cube, to cope well with the intensity variation in 3-D space. It can detect any branches including backwardly outgoing ones and provide a simple and easy way to correct erroneous segmented branches based on a tree-structured result.

The article is organized as follows: In Section II, we explain the proposed algorithm based on local cube tracking in detail. Then, Section III shows experimental results for various medical image datasets. Finally, conclusions are given in Section IV.

II. PROPOSED ALGORITHM

A. Overall Procedure. The proposed algorithm adaptively builds and segments successive local cubes, one by one. And, for the segmentation in each local cube, a region growing technique is adopted. The overall flow-chart for the proposed algorithm is shown in Figure 2, and related notations are as follows:

LC_{ij} The ith local cube of the jth branch

$$\{(x, y, z) | xm_{i,j} \le x \le XM_{i,j}, ym_{i,j} \le y \le YM_{i,j}, zm_{i,j} \le z \le ZM_{i,j}\},$$

where xm_{ij}, ym_{ij}, zm_{ij} XM_{ij}, YM_{ij} and ZM_{ij} are decided adequately for each local cube.

LC_{oo} Initial local cube determined by the user-given seed point

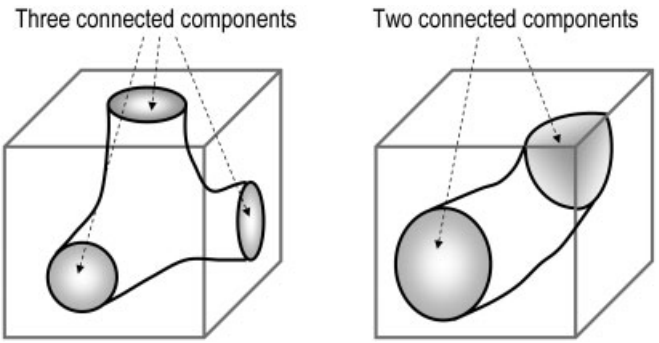

Figure 4. Examples of connected component labeling on the six cube-faces.

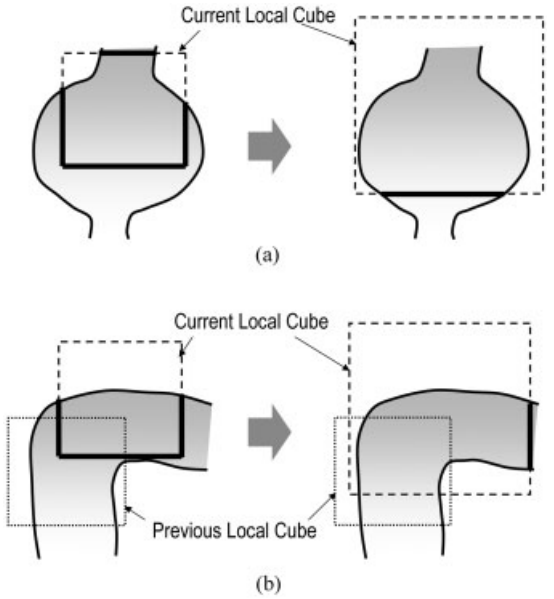

Figure 5. Examples of where the rule for a proper LC does not hold; (a) abrupt change in size and (b) wrong estimation of local cube position. They are depicted in 2-D space for simplicity.

{BQ}	Branch queue, storing newly branching local cubes
$LC_{ij} \rightarrow \{BQ\}$	Operation to push a local cube to the branch queue
$LC_{oj} \leftarrow \{BQ\}$	Operation to pop a local cube from the branch queue
bc	Branch count (Number of detected branches since the process begins)

First, to determine the initial local cube, LC_{00}, the vessel area is selected around the user-given seed point at the slice, by using a simple threshold-based method. Then, the center of LC_{00} is placed at the user-given point and the length of every edge is set to double the diameter of the selected vessel area. As shown in Figure 2, the

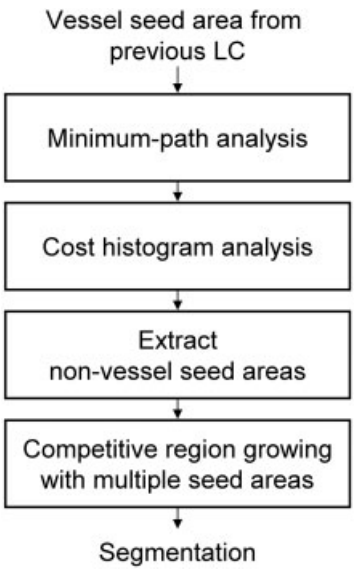

Figure 6. Proposed locally adaptive region growing scheme.

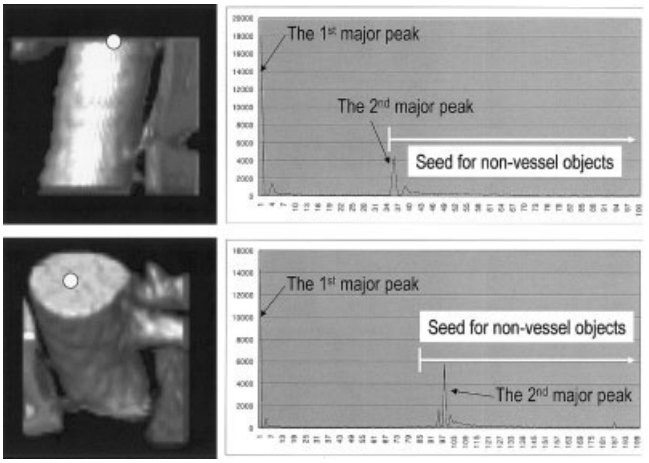

Figure 7. Two typical local cubes and their corresponding cost histogram graphs. Here, seed locations are marked with white circles.

iterative procedure begins from LC_{00} and is applied repeatedly to succeeding local cubes. At each procedure, after a local cube of the proper size is determined, vessel segmentation and branch detection are performed in it. Then, the positions of next local cubes are estimated based on connected component labeling, which will be described in detail in the next subsection. Here, each connected component is regarded as a seed area of each next local cube. Among the detected next local cubes, one local cube is chosen as a successor and the others are put to the branch queue {BQ} for later processing. If no next local cube is found in the current one, the processing for the current branch stops and the processing for a new branch begins by popping a local cube from the branch queue {BQ}. The whole procedure finishes when no more local cubes remain in the branch queue {BQ}. The local tube tracking procedure in 2-D space is depicted in Figure 3.

B. Branch Detection and Next Local Cube Selection. Now let us consider a proper selection of the positions and sizes of next local cubes. We first assume that vessel segmentation in the current local cube is properly performed by a localized region growing process. Then, to detect positions of next local cubes, we perform connected component labeling on the six faces of the current local cube. Because adjoining faces of a cube are regarded as being connected to each other, a connected component may span two or three adjoining faces. Figure 4 shows two examples of connected

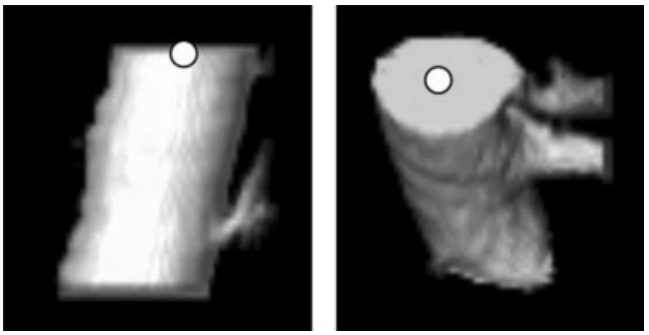

Figure 8. Voxels whose cost values are close to zero. They represent the object vessel well.

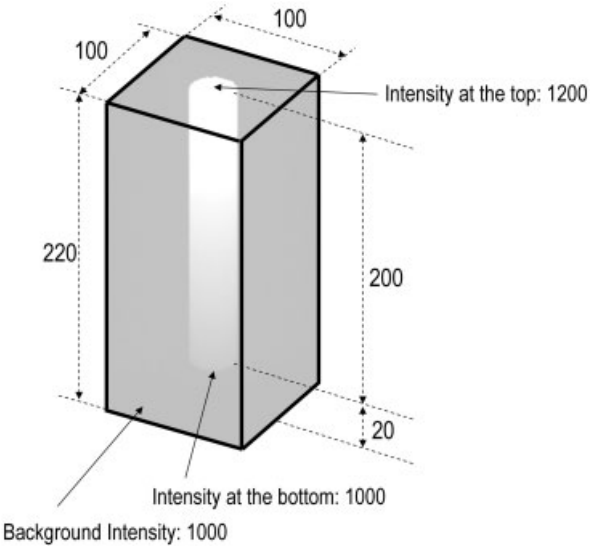

Figure 9. The shape of phantom.

component labeling on six cube-faces, which have three and two connected components, respectively. By examining the results from the connected component labeling, we can detect all branches in the current local cube and estimate the positions of next adjacent local cubes. The local cube, which corresponds to the component having

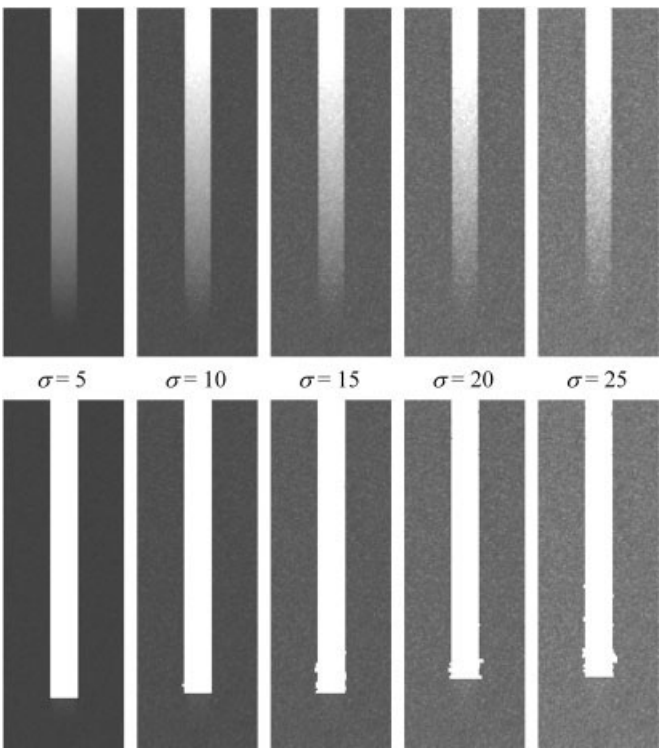

Figure 10. Experimental results for phantom data sets. Upper figures are MIP images of original phantom data sets added with Gaussian noises. Lower figures are MIP images of corresponding segmentation results. Standard deviation of Gaussian noise, σ, varies from 5 to 25.

Table I. Results for phantom data sets.

Noise Standard Deviation	The Slice at which the Segmentation Stops	Critical CNR
$\sigma = 5$	188	2.40
$\sigma = 10$	179	2.10
$\sigma = 15$	169	2.07
$\sigma = 20$	152	2.40
$\sigma = 25$	149	2.04

the largest number of labeled points, is chosen as a successor for the current branch, and the others are pushed into the branch queue {BQ} for later processing.

To estimate the proper positions of next local cubes, let C_i denote the center position of the current local cube, S_j the jth connected component, and $\{p_k \in S_j\}$ the points belonging to S_j. Then, we decide the center position of the next local cube, $C_{i+1,j}$ as follows:

$$C_{i+1,j} = \alpha \cdot \frac{1}{Card(S_j)} \sum_{Pk \in Sj} (p_k - C_i) + C_i, \qquad (1)$$

where α is a constant and $Card(S_j)$ denotes the number of points belonging to S_j. Here, the value of α is set to 1.2 in order to overlap next local cubes with the current one. The size of a next local cube is determined so that it may include the corresponding connected component, S_j. Then, its seed area is set to S_j. The next local cube with the position and size determined above may not be proper for branch detection. This could occur due to abrupt vessel size change as in an aneurysm or the sharp bending of a vessel (see Figure 5). To avoid this problem, the cube after region growing must satisfy the following rule:

Rule for a proper LC:

A single component cannot span on both of the opposite faces of the local cube simultaneously.

If any connected component does not satisfy the rule above, the result from the region growing is discarded and the local cube is enlarged twice in each direction and the region growing performed again.

C. Locally Adaptive Region Growing. For vessel segmentation in each local cube in Figure 2, a locally adaptive region growing scheme is adopted. Usually, region growing schemes are classified into two categories; single-seeded and competitive region growing. A single-seeded region growing scheme begins from a single kind of seed points in an object and grows them by merging their neighboring points until a predefined measure is met (Adams and Bischof, 1994; Hojjatoleslami and Kittler, 1998; Gonzalez and Woods, 1993). On the contrary, a competitive region growing scheme (Meyer and Beucher, 1990) begins from multiple kinds of seed points and grows them simultaneously until all the points are merged into one of the seeds. Although the competitive scheme produces

Table II. Dimension and resolution of the test images.

	Dimension	Resolution (mm)
CTA body	$512 \times 512 \times 416$	$0.66 \times 0.66 \times 1.00$
CTA carotid	$512 \times 512 \times 80$	$0.28 \times 0.28 \times 1.00$
MRA head	$512 \times 512 \times 200$	$0.39 \times 0.39 \times 0.60$

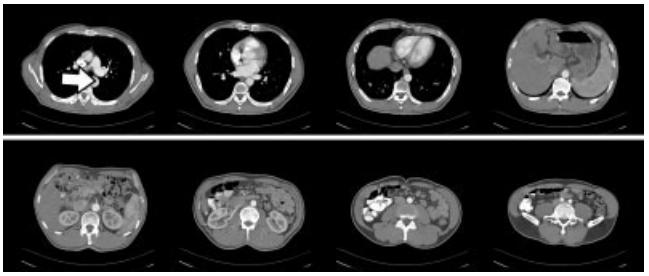

Figure 11. Several slice images selected from the original CTA data.

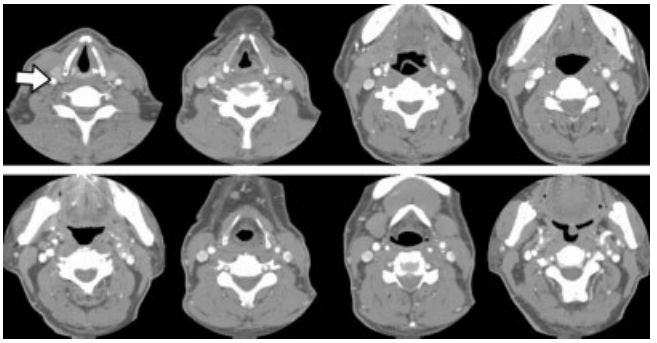

Figure 13. Several slice images selected from the CTA carotid data.

better-defined object boundaries, a proper seed area for every homogeneous object must be extracted in advance. Figure 6 depicts the flow diagram of the proposed scheme, which consists of nonvessel seed extraction based on a minimum path histogram and competitive region growing for segmentation.

From the viewpoint of local cube tracking, we use the segmented vessel from the previous local cube as a seed area for the vessel object in the current local cube. Based on the seed area, we calculate a cost, $Cost(p)$, on every point p in the cube. Let $PS_k(p, q)$ be the path-strength value along a path connecting two points, p and q, and an ordered list $P_k = \{p_o = p, p_1, \ldots, P_N, P_{N+1} = q\}$ be a path connecting p and q. Then, $Cost(p)$ can be computed as follows:

$$Cost(p) = \min_{k,s\varepsilon Seed} \{PS_k(p, s)\}, \tag{2}$$

$$PS(p, q) = \sum_{i=0}^{N} Diff(p_i, p_{i+1}),\ p_0 = p,\ p_{N+1} = q, \quad p_i \in P_k, \tag{3}$$

$$Diff(p_i, p_{i+1}) = \begin{cases} |I(p_i) - I(p_{i+1})|, & \text{if } |I(p_i) - I(p_{i+1})| > Th \\ 0, & \text{otherwise} \end{cases}, \tag{4}$$

where $I(p)$ denotes the intensity value at point p. We empirically set Th to 3, even though it is found that the final segmentation result is not so sensitive to its value. The procedure to compute a cost value, $Cost(p)$, on every point p can be efficiently implemented using a dynamic programming technique (Saha et al., 2000; Lei et al., 2000; Cormen et al., 1994).

Two typical local cubes from a 3-D CT angiographic data and the corresponding cost histogram graphs are shown in Figure 7. Note that the upper image includes unwanted spine nearby in addition to the object vessel, and the lower one includes another vessel as well as the spine. It should be noticed that cost values of the voxels inside the vessel of interest tend to be close to zero since an anatomical structure usually has homogeneous intensity values in a localized region. On the contrary, cost values outside the vessel become larger

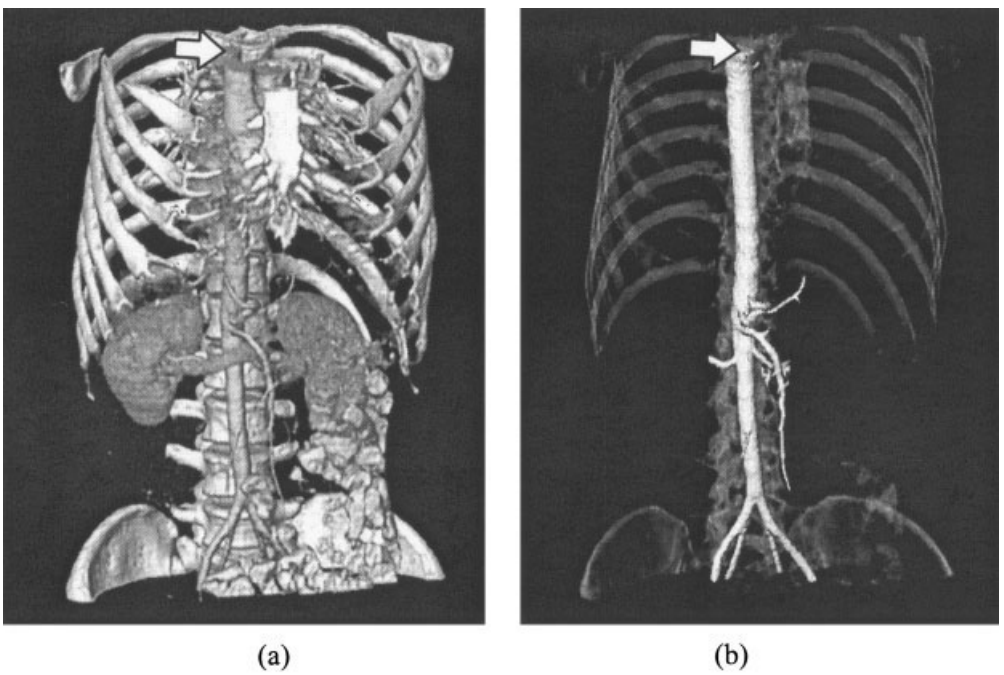

Figure 12. (a) A volume-rendered image of original CTA body data. (b) The segmented result is overlaid on a semi-transparent image.

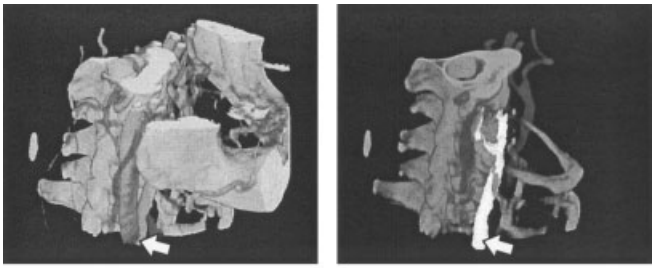

Figure 14. (a) A volume-rendered image of the CTA carotid data. (b) The segmented result is overlaid on a semi-transparent image. Here, the jawbone is manually removed to effectively demonstrate the segmented result. Note that the segmented vessel shows stenoses caused by calcification.

owing to intensity differences across region boundaries. Each image in Figure 8 shows the voxels whose cost values are closed to zero. As expected, selected voxels represent the object vessel. By using a cost histogram graph in Figure 7, two major peaks can be automatically detected and used to select a threshold value for extracting nonobject seed areas. By using the extracted nonobject seed areas and the tracked vessel as the object seed area, competitive region growing is performed to segment the current local cube. Notice that the computing time for cost values at all points is not so heavy because the procedure is confined to a small localized volume.

D. Tree-structured Segmentation. In the proposed algorithm, the parent-child relationships between local cubes are stored for later use. Therefore, a tree-structured segmentation result can be obtained by giving each detected branch a unique label. Also, a user can easily correct the segmentation result by adopting a pruning-strategy (branch-by-branch removal), if needed. In addition, the centerlines of the vessel structure can be approximated by connecting the center positions of local cubes, and can be used in various applications, such as automatic flyway generation in a virtual angioscopy system.

III. EXPERIMENTAL RESULTS

In the experiment, we use a phantom whose shape is shown in Figure 9. In the phantom, a pipe (or a vessel) is located at the center through upper 200 slices out of 220, where the intensity value is gradually decreasing from 1200 to 1000 and the background intensity is fixed to 1000. And zero-mean Gaussian noises with various standard deviations, from $\sigma = 5$ to $\sigma = 25$, are added. Here, these

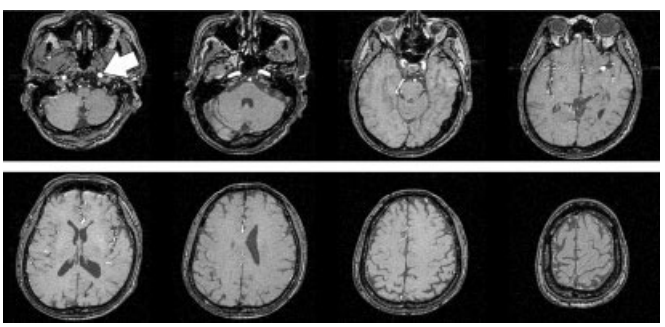

Figure 15. Several slice images selected from the MRA head data.

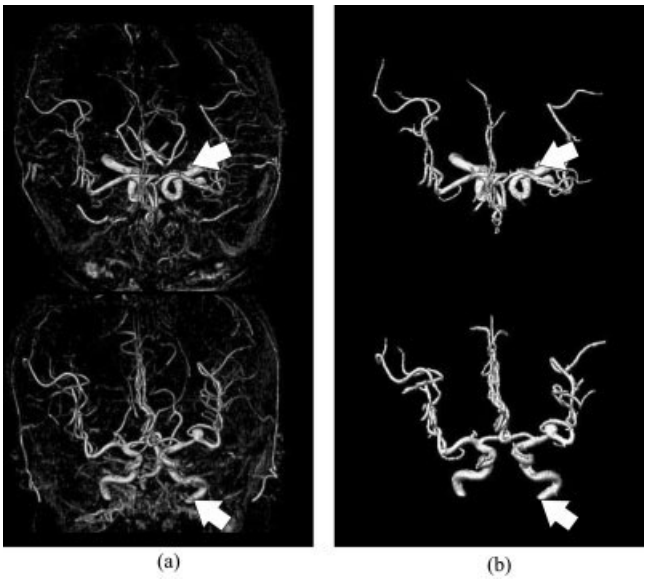

Figure 16. Volume-rendered images at two different view directions for (a) the MRA head data and (b) its segmented result.

values are regarded to cover the range of noise levels in real medical images. The seed point for the first local cube is assumed to be placed on the top slice. The upper row of Figure 10 shows maximum-intensity projection (MIP) images of the phantom for various σ and the lower one shows the corresponding segmentation results. To evaluate the performance of the proposed method, we adopt the contrast-to-noise ratio (CNR) that is defined by

$$CNR(n) = \frac{contrast(n)}{\sigma}. \tag{5}$$

Here, the *contrast*(n) is the intensity difference between the pipe and background at a slice, n, in the original phantom. Because the segmentation proceeds from the top slice where the CNR value is the maximum, we can evaluate the performance of the proposed method by calculating the CNR value (or critical CNR) on the slice at which the segmentation stops. Here, the slice at which the segmentation stops is the first slice that the number of erroneously segmented pixels becomes more than 20% of pixels in pipe. Table I shows the slices at which the segmentation stops depending on various σ and the corresponding critical CNR values. It should be

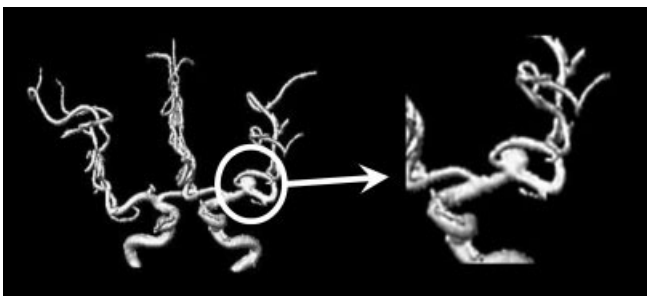

Figure 17. Volume-rendered images for segmentation at an aneurysm in the MRA head data.

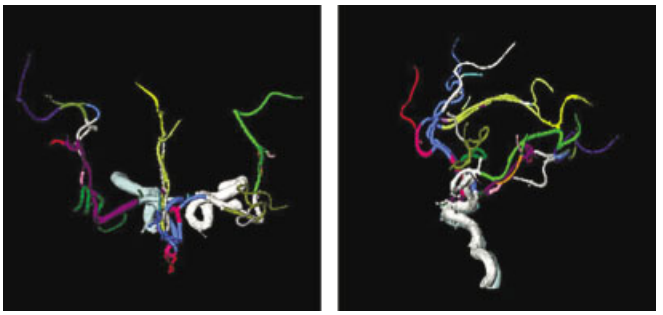

Figure 18. Branch-by-branch labeling for a segmentation result of MRA head data.

noticed that the critical CNR values are in the range of 2.04 to 2.40. Hence, the proposed method can segment an object well unless the contrast between the object and background is less than about two times of the noise standard deviation.

In the experiment for real images, we use the three different sets of data: CTA body images, CTA carotid images, and MRA head images. Dimensions and resolutions of the sets are listed in Table II. Parts of these images are shown in Figures 11, 13, and 15, respectively. For segmentation, the seed point for the first local cube is given by a user. Also, the parameters, α in Eq. (1) and Th in Eq. (4), are kept the same irrespective of images. In Figures 12, 14, and 16, volume-rendered images of the original image sets and their segmentation results are given in the left and right sides, respectively. Here, white arrows represent user-selected initial points. It is noted that the proposed algorithm can provide good and robust segmentation results for all three data sets of vascular structures. Compared to existing algorithms, the proposed algorithm provides the robust results for the vessels having slowly varying intensities and can detect fairly thin branches including even backwardly outgoing branches. Also, the results comprise abnormalities, such as stenoses shown in Figure 16 and aneurysms shown in Figure 17. It is also interesting to note that, because the proposed algorithm divides the segmentation results into branches, different colors can be assigned to different branches without additional computation (see Figure 18). Thereby, the result can be easily edited, if necessary.

The computation time is 22 sec for CTA carotid images, 37 sec for MRA head images and 4 min 48 s for CTA body images, measured on a standard PC with a CPU of 1.63 GHz. It is noticeable that the CTA body images require more processing time compared to the other cases. This is mainly because some local cubes grow bigger because of improper segmentation (see subsection II.B) and big local cubes require much time in the minimum path analysis. Therefore, a better scheme to predict the position and size of next local cubes in the branch detection may reduce the chance of improper segmentation, thereby reduce the whole processing time.

IV. CONCLUSIONS

In this article, we propose a vessel segmentation algorithm based on local cube tracking. The algorithm segments the vessel in the subsequent local cubes iteratively, starting from the initial local cube determined by a user-selected point. Thereby, it provides prospective results even for a long vessel structure with slowly varying intensity. Contrary to existing algorithms, the proposed algorithm can detect most branches in any direction, whereas the computation complexity is small compared to various model-based approaches.

REFERENCES

R. Adams, and L. Bischof, Seeded region growing, IEEE Trans Pattern Anal Machine Intell 16 (1994), 641–647.

A. Bhalerao, E. Thönnes, W. Kendall, and R. Wilson, Inferring vascular structure from 2D and 3D imagery, Proc MICCAI 2001 LNCS 2208, 2001, pp. 820–828.

T. Cormen, C. Leiserson, and R. Rivest, Introduction to algorithms, MIT Press, New York, 1994.

P. Felkel and R. Wegenkittl, Vessel tracking in peripheral CTA datasets—An overview, VRVis Technical Report 2001-009, 2001.

M. Fiebich, M.T. Mitchell, R.M. Engelmann, and K.R. Hoffmann, Automatic segmentation in CT angiography of the abdominal aorta, Proc Comput Assisted Radiol Surg (1997), CAR '97, 277–282.

N. Flasque, M. Desvignes, J.M. Constans, and M. Revenu, Acquisition, segmentation and tracking of the cerebral vascular tree on 3D magnetic resonance angiography images, Medical Image Analysis 5 (2001), 173–183.

J.D. Furst, S. Pizer, and D. Eberly, Marching cores: A method for extracting cores from 3-D medical images, Proc Workshop Mathematical Methods Biomedical Image Analysis, 1996, pp. 124–130.

S.A. Hojjatoleslami and J. Kittler, Region growing: A new approach, IEEE Trans Image Processing 7 (1998), 1079–1084.

R.C. Gonzalez and R.E. Woods, Digital image processing, Addison-Wesley Publishing Co., New York, 1993.

T. Koller, G. Gerig, G. Székely, and D. Dettwiler, Multiscale detection of curvilinear structures in 2-D and 3-D image data, Proc the Fifth Int Conf. on Computer Vision, 1995, pp. 864–869.

K. Krissian, G. Malandain, and N. Ayache, Model based multiscale detection of 3D vessels, Proc Workshop on Biomedical Image Analysis, (1998), 202–208.

T. Lei, J.K. Udupa, P.K. Saha, and D. Odhner, Separation of artery and vein in contrast enhanced MRA images, Proc SPIE Medical Imaging 978, (2000), 233–244.

C. Lorenz, I-C. Carlsen, T. M. Buzug, C. Fassnacht, and J. Weese, Multiscale line segmentation with automatic estimation of width, contrast and tangential direction in 2D and 3D medical images, Proc CVRMed and MRCAS LNCS 1205, (1997), 233–242.

F. Meyer and S. Beucher, Morphological segmentation. J Visual Comm Image Representation 1 (1990), 21–46.

T. O'Donnel, A. Gupta, and T. Boult, A new model for the recovery of cylindrical structures from medical image data, Proc CVRMed and MRCAS LNCS 1205, (1997), 223–232.

V. Prinet and O. Monga, Vessel representation in 2-D and 3-D angiograms, Proc Comput Assisted Radiol Surg (1997), CAR '97, 240–245.

P.K. Saha, J.K. Udupa, and D. Odhner, Scale-based fuzzy connected image segmentation: Theory, algorithms, and validation, Comput Vision Image Understanding 77 (2000), 145–174.

D. Terzopoulos, A. Witkin, and M. Kass, Constraints on deformable models: Recovering 3-D shape and nonrigid motion, Artific Intelli 36 (1988), 91–123.

B. Verdonck, I. Bloch, H. Maître, D. Vandermeulen, P. Suetens, and G. Marchal, Accurate segmentation of blood vessels from 3-D medical images, Proc Int Conf of Image Processing (1996), 311–314.

D.L. Wilson and J.A. Noble. An adaptive segmentation algorithm for time-of-flight MRA data, IEEE Trans Med Imaging 18 (1999), 938–945.

O. Wink, W.J. Niessen, and M.A. Viergever, Fast delineation and visualization of vessels in 3-D angiographic images, IEEE Trans Med Imaging 19 (2000), 337–346.